An Ultra-Low Power Closed-Loop Distributed Beamforming Technique for Efficient Wireless Power Transfer

Ankit Mittal, *Student Member,* S. Shiva Kumar

Abstract—This paper presents a clphase correction technique for distribut imize the wireless radio frequency (F multiple energy transmitters (TX) to a device receiver (RX). A mathematical power loss due to frequency and phase transmitters, is used to establish a des quency and phase correction among n-i quantifies the received signal power in and phase offsets and shows that an opt correction can boost the combined sig of n^2 from *n*-transmitters. Further, we p which can expedite the phase offset corr one-shot phase correction algorithm. frequency and phase offset correction a 9.5 dB improvement in received po using Universal Software Radio Periph commercial rectifier at 2.4 GHz for a di

TX and RX. Our proposed closed-loop correction technique utilizes backscatter communication between TX and RX, which improves the energy efficiency of the distributed beamforming system.

Index Terms—RF energy harvesting, wireless power transfer, distributed beamforming, multi-transmitter, power combining, ultra-low power IoT, phase correction, backscatter communication.

I. Introduction

White the proliferation of Internet-of-things (IoT) devices in our environment [1], the amount of ambient radio frequency (RF) energy will continue to increase [2]. This will continue to enable more and more IoT applications being powered by ambient RF energy [3]–[5], increasing the otherwise limited lifespan of conventional energy-constrained wireless IoT devices. Given the relatively low power density of ambient RF signals [6], [7], a large body of research has focused on enhancing the power conversion efficiency [8]–[11]. However, more energy can be obtained by harvesting from the distributed RF transmitters that are now readily available.

To harvest higher overall energy, there has been a move towards harvesting RF energy from diverse sources like

A. Mittal, Z. Xu, K. Du and A. Shrivastava are with the Department of Electrical and Computer Engineering, Northeastern University, Boston, MA, 02115 USA. e-mail: ({mittal.ank, xu.ziy, du.kad}@northeastern.edu, aatmesh@ece.neu.edu.)

S. Shiva Kumar is with the Department of Electrical & Electronics Engineering, BIT Mesra, Ranchi, Jharkhand, India. email: (shivkumar.ee@bitmesra.ac.in).

The work in this paper is supported in part by National Science Foundation (NSF) under grant nos #CCSS-2225368 and #RINGS-2146754 with funds from OUSD R&E, NIST, and industry partners as specified in the Resilient & Intelligent NextG Systems (RINGS) program.

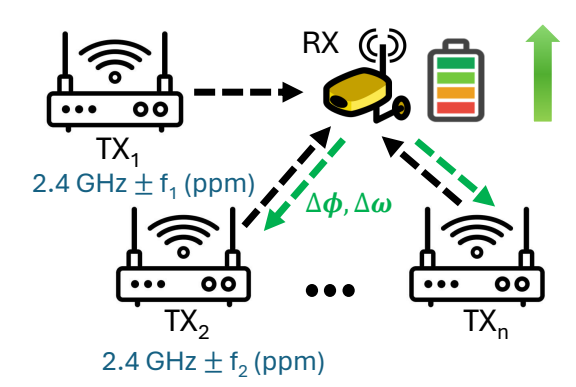


Fig. 1. An optimal RF energy harvesting requires frequency and phase offset correction between the transmitters.

broadband [12]–[14], multi-band [15]–[17], and multi-antenna setups [18]–[22] apart from refining underlying RF rectifier circuits. Compared to utilizing multiple antennas, harvesting RF energy from multiple transmitters (TX) is emerging as a promising technique, well-suited for real-world scenarios involving widespread IoT sensors. This technique helps in keeping the size of the IoT sensor smaller as incorporating array antennas into IoT sensors faces size limitations [23], [24].

Distributed beamforming, an approach where energy from spatially distributed transmitters can be beamformed at a far-off energy receiver [25], is a promising solution for RF energy harvesting particularly with the growing distribution of RF transmitters in our surroundings. Fig. 1 illustrates the distributed RF energy harvesting for the IoT device from multiple transmitters. IoT receiver (RX) functions as the energy receiver, gathering RF energy from various sources. While RF distributed beamforming from dedicated RF transmitters can enhance received signal power, our vision is to utilize ambient RF transmitters to achieve distributed beamforming.

Due to the physical placement and diverse transmitter types, the received signal strength suffers not only from free space path loss but also from phase offsets caused by distinct propagation paths. Apart from phase misalignment, frequency tolerances (offset) among transmitters even at same RF channel is common. Tolerances within ±20 to ±40 partsper-million (ppm) are specified in popular IEEE standards like 802.11 [26]. These tolerances originate from manufacturing tolerances of reference clock crystal resonators (XO), which ultimately generates phase-locked loop (PLL) to generate the local oscillators (LO). Both phase and frequency offset will result in loss in received RF power at RX. In Fig. 1, we visualize a scenario where frequency and phase offset exists

1

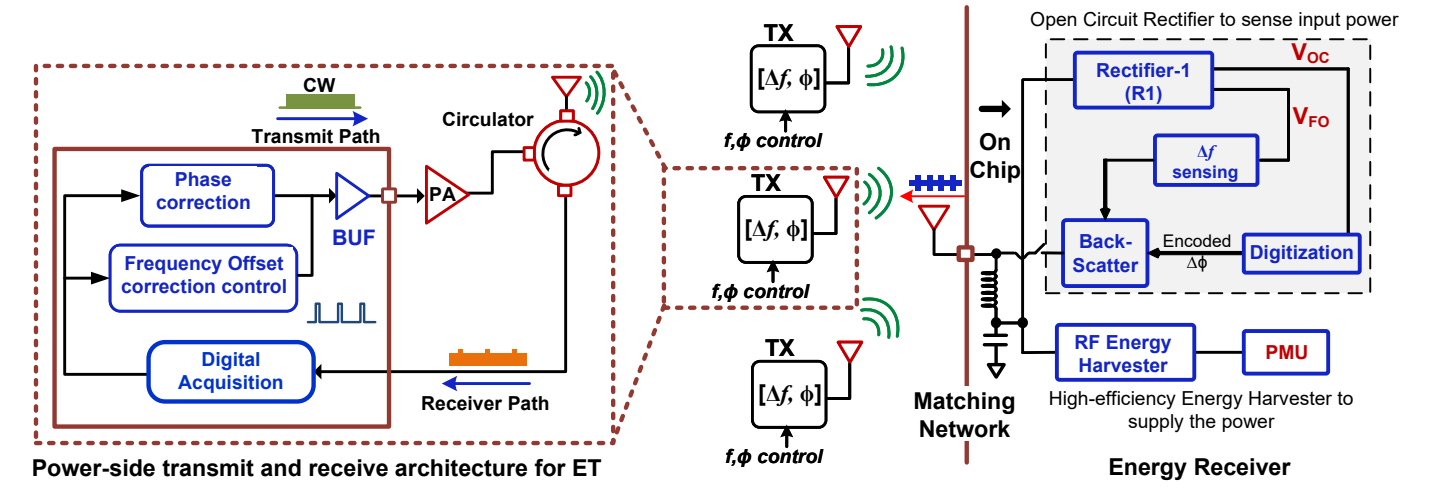


Fig. 2. System architecture for the proposed closed-loop beamforming for frequency and phase offset correction between the transmitters to maximize received signal at the ULP energy receiver.

between the transmitters. Correcting for the frequency and phase offset can boost the received signal power at the RX. Consequently, this underscores the need for frequency-phase offset correction techniques to facilitate effective distributed beamforming [27].

Common techniques for phase synchronization involve employing algorithms like the one-bit feedback algorithm [28]. [29]. This method continuously seeks optimal phase alignment using feedback, resulting in maximizing received power but at the expense of extended peak convergence time and increased power overhead. Various system-level studies [25], [30], [31] have focused on addressing frequency offset issues. In [31], authors proposed an open-loop distributed beamforming system employing a self-mixing circuit for frequency synchronization. This system transmits a reference signal to sensors, which then feeds into a phase-locked loop (PLL) to synchronize the local oscillator. However, lacking a feedback mechanism makes managing time slots intricate, particularly with a larger number of sensors. Similarly, [30] introduced a master-slave architecture to expedite the recognition of reference signals from the master sensor to the slave sensors. Nonetheless, the assumption of significant signal processing capability at the receiver, which involves higher power consumption, conflicts with the energy constraints of wireless powered sensors. Achieving optimal energy harvesting from multiple transmitters necessitates an ultra-low power (ULP) hardware solution that operates in a closed-loop manner, efficiently addressing phase and frequency offsets.

In this paper, we introduce a closed-loop RF wireless power transfer (WPT) scheme operating at 2.4 GHz, incorporating both phase and frequency correction techniques. By correcting both frequency and phase offsets, we can boost the signal strength using an ULP received power sensing technique. We employ a backscattering communication technique to enable closed-loop feedback-based correction. These techniques enable a closed-loop beamforming with a power overhead in 10s of nano-watts, reducing power by a few orders of magnitude to enable a high efficiency distributed beamforming WPT.

We summarize the main contributions of this paper as

follows:

- A ULP received power sensing technique using onchip passive rectifiers, low-power sensing circuits, and a backscattering communication method is proposed to lower the power, cost, and size associated with closed loop beamforming.
- It presents a detailed analysis and simulation results for the received power loss due to the frequency and phase offset among n-transmitters.
- It presents an optimization technique using a one-shot algorithm to achieve a faster phase offset correction.
- A demonstration of the proposed phase and frequency correction techniques at 2.4 GHz is carried out using commercial Universal Software Radio Peripheral (USRP) software defined radios (SDR).

The rest of paper is organized as follows. In Section II, we present the system architecture for distributed beamforming. In Section III, we present a detailed analysis of power loss due to frequency and phase offset for *n*-TX. Section IV presents simulation results of the proposed correction techniques and establishes the optimal conditions for frequency and phase offset correction technique. In Section V, we present measurement results of the distributed wireless beamforming using USRP SDR and a commercial rectifier. Finally, conclusions are presented in Section VI.

II. SYSTEM ARCHITECTURE

Fig. 2 shows the architecture of the proposed closed-loop, RF distributed beamforming energy harvesting system. On the energy receiver side, it consists of the RF-to-DC rectifier, frequency offset sensing circuit, digitization block, and backscatter communication system. An envisioned ULP (nano-watts) power sensing technique is proposed to sense the received power level implemented with a high-efficiency rectifier [8], [9], [32] which maximizes conversion efficiency for RF to DC conversion and a ULP backscattering communication method is used to close the loop for continuous frequency and phase correction. The ULP sensing of incoming power is performed using an open-circuit rectifier in combination

with an analog to digital converter (ADC). A backscattering technique is used to send short pulses to transmit the received power information for aligning transmitter phases. On the transmitter side, the coupler senses the returned back-scattered on-off-keying signal, which then undergoes digital acquisition. Based on our analysis in Sections IV.A and IV.C, frequency offset correction will be performed first by introducing an N-point phase shift keyed transmit power. After the frequency correction, the phase offset is extracted and compensated for with a one-shot correction technique. In Table I, we present an estimated power consumption of different blocks to be used in our ULP energy receiver. The optimal beamforming technique will realize maximum power for the energy receiver.

A. Frequency and Phase Sensing Technique

Small frequency offset exists among transmitters due to LO offsets, even at the same channel. With a frequency offset of Δf between two transmitters, the received power becomes $A^2 + B^2 + 2AB\cos(2\pi\Delta ft + \phi)$, which results in a reduced power due to loss of phase alignment. To continue to harvest maximum power, the $2\pi\Delta ft + \phi = 0$ condition needs to be fulfilled; i.e., requiring phase to continuously adjust and track Δf , similar to introducing a phase-shift keying modulation. We use binary phase shift keying (BPSK) to correct for the frequency offset. We aim to feedback the level of received power to optimize beamforming. The proposed power sensing technique will sense the level of received power to obtain the phase and frequency offset information among transmitters in a pairwise manner. It will then communicate through feedback using the ULP backscatter communication technique. We propose to remove the frequency offset by periodically changing the phase of one transmitter relative to the other. The feedback from the energy receiver will provide the value of Δf , which will be used to synchronize the frequency of the LO.

B. Backscatter Communication

Backscattering transmission, which is commonly used in radio frequency identification (RFID) and near-field communication (NFC), is now also being considered for wireless communication due to its low power transmission [33]–[38]. In the very basic form, backscattering transmitters modulate the impedance of the antenna to change the reflection coefficient based on the binary bits it intends to transmit. Due to the modulated impedance, the incoming continuous wave (CW) is reflected back to the base station differently and can be recovered. However, due to the two-way transmission path-loss, multi-path induced fading, and self-jamming from the basestation transmitter, the range of backscattering communication is rather limited. Recent works aim to address self-jamming issue by using intermediate frequency (IF) modulation to move the backscattered signal to an alternate channel [35], [37]. However, the use of IF modulation frequency at several MHz increases its power consumption to $28\mu W$ [35] or $113\mu W$ [37], which is still quite high to enable useful RF energy transfer. In WPT application, particularly in closed-loop beamformed RF energy harvesting as presented in this paper,

TABLE I
POWER CONSUMPTION OF DIFFERENT DESIGN BLOCKS USED IN THE
PROPOSED ULP ENERGY RECEIVER.

Design Block	Power (nW)	Ref.
Rectifier	0	[32], [39], meas*
Δf sensing (Comparator)	< 10	[40], [41], meas*
Digitization (ADC)	< 20	[42]–[44]
Backscatter	< 1	sim**
Total	< 30	-

^{*} Measurement using a 65-nm CMOS chip, ** design simulation using 65-nm CMOS technology.

the energy transmission requirements and application scenario varies from a conventional data transmission in several ways. (i) In wireless power transmission, the energy transmitter needs to continuously send power for a considerable duration such that the energy receiver can harvest sufficient energy. (ii) The impedance modulation of antenna adversely affects the harvested energy as it will move the antenna from its matched configuration resulting into an increased reflection of the received power. (iii) Assuming beamforming can realize higher incident power, backscattering inherently is set up for longer range as it will reflect at higher power level. On the energy receiver side, received power information is sent to the backscattering transmitter, which uses on-off keying (OOK) to send short and fixed time backscattering pulses. On the energy transmitter side, these backscattering pulses are received and demodulated to recover the phase and frequency offset information, which is then used to configure the phase and delay of the LO.

C. Energy Harvesting RF-to-DC Rectifier

An efficient RF-to-DC converter (rectifier) is an important component in the energy receiver as it serves a dual purpose: First, it operates as a passive RF energy detector by utilizing open circuit output voltage to represent received signal strength. By configuring the output capacitor, the frequency offset can also be extracted to facilitate frequency correction. Second, the rectifier works as the RF energy harvester to harvest ambient RF energy. Classical Dickson multiplier is analyzed and improved by [45], [46] in terms of the efficiency and sensitivity. In Fig. 2, the energy harvester operates with correct impedance matching when we are harvesting. We utilize the RF-switch for backscattering communication which changes the impedance matching causing the power to be reflected back which can be received at the transmitter. The short pulses are used to communicate using backscattering so that impedance matching is maintained most of the time for energy harvesting. While our proposed closed-loop correction technique aims to maximize received RF energy, the effectiveness of the ULP energy receiver depends upon ensuring an effective conversion of this received RF energy into DC. These considerations emphasize the need for an RF-to-DC rectifier that achieves high efficiency and sensitivity in low power scenarios, allowing for exploration of the lowest detectable power while efficiently utilizing available power [32]. Furthermore, an increased rectifier sensitivity has the potential to extend

TABLE II PARAMETER DESCRIPTION.

Parameter	Details
T	Time duration for distributed beamforming
A_i	Transmit signal amplitude of the i th TX
ω	Carrier frequency of the TX signal
φ	TX Phase
Δω	Frequency offset between TXs
$\Delta \phi$	Phase offset between TXs

the effective operational range for scenarios involving multiple transmitters.

III. PHASE AND FREQUENCY OFFSET ANALYSIS

To quantitatively assess the loss in the received power, we present a detailed analysis for the distributed beamforming, under the effect of frequency and phase offset, in the network of *n*-TX. Each TX is sending a continuous (CW) signal within the same RF band (2.4 GHz). Although the transmitters operate within the same RF band, the signals they emit exhibit variations due to frequency and phase offsets and as such signals are different. The combined received power from *n*-TX when received at the energy receiver can be written as:

$$V_{o,n-TX}(t) = \sum_{i=1}^{N} A_i cos(\omega t + \Delta \omega_i t + \phi_i), \tag{1}$$

where $\Delta\omega_i$ and ϕ_i represent the frequency offset and phase offset respectively for the i^{th} transmitter.

A. Analysis for 2-TX system

We begin our analysis by considering 2-TX (n=2), and then subsequently extend it to n-TX.

$$V_{o,2-TX}(t) = A_1 cos(\omega t + \alpha_1(t)) + A_2 cos(\omega t + \alpha_2(t)),$$
 (2) where $\alpha_1(t) = \Delta \omega_1 t + \phi_1$ and $\alpha_2(t) = \Delta \omega_2 t + \phi_2$ Simplifying (2), we get

$$V_{o,2-TX}(t) = \underbrace{\sqrt{A_1^2 + A_2^2 + 2A_1 A_2 cos(\Delta \alpha_{1,2}(t))}}_{Signal\ envelope} \cdot cos(\omega t + \theta),$$
(3)

where $\Delta \alpha_{1,2}(t) = (\Delta \omega_1 - \Delta \omega_2)t + (\phi_1 - \phi_2) \implies (\Delta \omega_{1,2})t + (\Delta \phi_{1,2})$ and,

$$\theta = tan^{-1} \left(\frac{A_1 sin\alpha_1(t) + A_2 sin\alpha_2(t)}{A_1 cos\alpha_1(t) + A_2 cos\alpha_2(t)} \right). \tag{4}$$

Average power $P_{avg|V_{o,2-TX}}$ of the combined signal $(V_{o,2-TX})$ (3) can be written as,

$$\begin{split} &P_{avg|V_{o,2-TX}} = \frac{1}{T} \int_{-T/2}^{T/2} V_{o,2-TX}^2(t) \, dt \\ &= \frac{1}{T} \int_{-T/2}^{T/2} \left(A_1^2 + A_2^2 + 2A_1 A_2 cos(\Delta \alpha_{1,2}(t)) \right) cos^2(\omega t + \theta) \, dt, \end{split}$$

where T represents the duration during which transmitters transmit wireless power for distributed beamforming, typically in the range of hundreds of milliseconds, depending on the application. Since the time duration of the sinusoid characterized by frequencies 2ω and $2\omega \pm \Delta\omega$ is much smaller than T (on the order of 10^9), the average of these sinusoids tends towards zero. The average power thus approaches the mean square value of the signal amplitude (envelope of the signal in (3)) . Solving this we get,

$$P_{avg|V_{o,2-TX}} = \frac{1}{2} (A_1^2 + A_2^2) + A_1 A_2 \cdot \beta(t), \tag{6}$$

where,

$$\beta(t) = \frac{1}{T} \int_{-T/2}^{T/2} \cos(\Delta \alpha_{1,2}(t)) dt.$$
 (7)

It should be noted that in (6), that we have retained the term represented by $\beta(t)$, which is $f(A_1, A_2, \Delta\omega_{1,2}, \Delta\phi_{1,2})$.

The term $cos(\Delta\alpha_{1,2}(t))$ in (7) is not strictly a sinusoidal function, and under special conditions, which we discuss below, transforms into a constant signal. Therefore, it cannot be directly treated as a sinusoidal signal while other terms are sinusoidal signals regardless of the value of θ (averaging to zero in the time period). Based on (6), we derive three scenarios, which gives us an insight into the power content of the combined signal and guides our frequency-phase correction technique for an efficient power transfer.

1) Case 1: $\Delta\omega_{1,2} \neq 0$ Finite frequency offset exists between the 1st and 2nd transmitter (regardless of the value of $\Delta\phi_{1,2}$). Solving (7), we see that the integral term for the sinusoid

vanishes and average power is given by:

$$P_{avg|V_{o,2-TX}} = \frac{1}{2} (A_1^2 + A_2^2).$$
 (8)

2) <u>Case 2</u>: $(\Delta\omega_{1,2} = 0 \text{ and } \Delta\phi_{1,2} \neq 0) \implies \alpha_{1,2}(t) = \Delta\phi_{1,2}$ Only phase offset exists between the 1st and 2nd transmitter. Average power of the signal is given by:

$$P_{avg|V_{0,2-TX}} = \frac{1}{2} \left(A_1^2 + A_2^2 \right) +$$

$$A_1 A_2 \cdot \left(\frac{1}{T} \int_{-T/2}^{T/2} \cos(\Delta \phi_{1,2}) dt \right)$$

$$= \frac{1}{2} \left(A_1^2 + A_2^2 + 2A_1 A_2 \cos(\Delta \phi_{1,2}) \right). \quad (9)$$

3) Case 3: $(\Delta\omega_{1,2} = 0 \text{ and } \Delta\phi_{1,2} = 0) \implies \alpha_{1,2}(t) = 0$ No frequency or phase offset exists between the 1st and 2nd transmitter (ideal case). Average power of the signal is given by:

$$\begin{split} P_{avg|V_{o,2-TX}} &= \frac{1}{2} \bigg(A_1^2 + A_2^2 + 2A_1A_2 \bigg) \\ &= \frac{1}{2} \big(A_1 + A_2 \big)^2. \end{split} \tag{10}$$

Following observations can be drawn from (8)–(10)

 From Case I, we observe that a frequency offset between transmitters manifests into independence of signals in the spectral space and regardless of the phase offset,

- they contribute independently to the average power of the combined signal.
- 2) Phase offset correction without frequency-offset correction does not improve the average power of the signal (8). This implies, that frequency offset correction must precede phase correction to improve the power of the combined signal.
- 3) From (9), we observe that once we correct for frequency-offset, the effect of phase offset manifests itself in the combined signal. Combined signal power, depending on the value of $(\Delta\phi_{1,2})$, can now vary from zero to the maximum power.
- 4) As the frequency-offset manifests itself as a *dynamic* phase offset $(\Delta\omega_{1,2}(t))$, hence we need to resort to a periodic-phase correction technique.

B. Analysis for n-transmitters

We now extend our analysis to n-TX

$$P_{avg|V_{o,n-TX}} = \frac{1}{T} \int_{-T/2}^{T/2} \left(\sum_{i=1}^{n} A_i cos((\omega + \Delta \omega_i)t + \phi_i) \right)^2 dt.$$
(11)

Solving this using square expansion of *n*-terms we get,

$$\begin{split} P_{avg|V_{out,n-Tx}(t)} &= \frac{1}{T} \left[\int_{-T/2}^{T/2} \left(\sum_{i=1}^{n} A_i^2 cos^2((\omega + \Delta \omega_i)t + \phi_i) \right) dt \right. \\ &+ \frac{1}{T} \left[\int_{-T/2}^{T/2} \left(2 \sum_{i=1}^{n} \sum_{i < j}^{n} \left(A_i cos(\omega_i t) \cdot A_j cos(\omega_j t + \Delta \phi_{i,j}) \right) dt, \right. \end{split}$$

where $\Delta \phi_{i,j}$ represents the phase difference between i^{th} and j^{th} transmitter

The first term represents average power of each of the signal at ω_i

$$P_{avg|V_{out,n-T_X}(t)} = \frac{1}{2} \left(\sum_{i=1}^{n} A_i^2 \right)$$

$$+ \frac{1}{T} \left[\int_{-T/2}^{T/2} \left(2 \sum_{i=1}^{n} \sum_{i < j}^{n} \left(A_i cos(\omega_i t) \cdot A_j cos(\omega_j t + \Delta \phi_{i,j}) \right) dt. \right]$$

$$(13)$$

The second term here represents the role of frequency and phase offset in the overall energy. If there is an offset such that $\omega_i \neq \omega_j$, then by condition of orthogonality the resultant term would be zero.

$$P_{avg|V_{o,n-TX},\omega_i \neq \omega_j} = \frac{1}{2} \left(\sum_{i=1}^n A_i^2 + 2 \sum_{i=1}^n |\vec{A}_i \cdot \vec{A}_j| \right). \tag{14}$$

We note that (14) is a more generic representation of the average power of combined signal. In case of frequency offset, the dot product of two uncorrelated vectors (independent spectral components, as discussed before) is zero and hence equation reduces to sum of square of amplitudes of different spectral components.

TABLE III PHASE AND FREQUENCY OFFSET SCENARIOS FOR n-TX DISTRIBUTED BEAMFORMING.

$\Delta \omega$	$\Delta \phi$	$P_{avg,min}$	$P_{avg,max}$	$P_{loss^*}(\%)$	$P_{gain}(dB)$
≠ 0	-	$\frac{1}{2} \left(\sum_{i=1}^{n} A_i^2 \right)$	$\frac{1}{2} \left(\sum_{i=1}^{n} A_i^2 \right)$	50	$10 \cdot \log(n)$
= 0	≠ 0	$\frac{1}{2} \left(\sum_{i=1, j \neq i}^{n} (A_i - A_j)^2 \right)$	$\frac{1}{2} \left(\sum_{i=1}^{n} A_i \right)^2$	(0-100)	$20 \cdot \log(n)$ (max)
= 0	= 0	$\frac{1}{2} \left(\sum_{i=1}^{n} A_i \right)^2$	$\frac{1}{2} \left(\sum_{i=1}^{n} A_i \right)^2$	0	$20 \cdot \log(n)$

^{*} $P_{loss} = (P_{avg,max} - P_{avg,min})/P_{avg,max}$

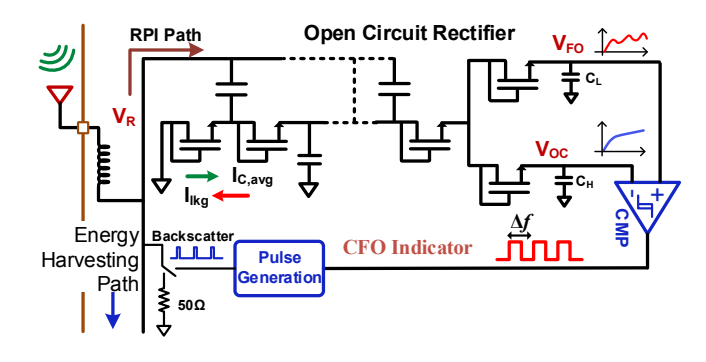


Fig. 3. Circuit architecture for sensing received power and frequency offset with ULP consumption.

Applying Cauchy-Schwartz inequality

$$P_{avg|V_{o,n-TX},\omega_{i}\neq\omega_{j}} = \frac{1}{2} \left(\sum_{i=1}^{n} A_{i}^{2} + 2 \sum_{i=1}^{n} \sum_{i< j}^{n} |A_{i}| |A_{j}| \right)$$

$$\leq \frac{1}{2} \left(\sum_{i=1}^{n} A_{i} \right)^{2}. \quad (15)$$

Therefore, the average power for n-TX has a range of,

$$\frac{1}{2} \left(\sum_{i=1, j \neq i}^{n} (A_i - A_j)^2 \right) \le P_{avg|V_{o, n-TX}} \le \frac{1}{2} \left(\sum_{i=1}^{n} A_i \right)^2. \tag{16}$$

Average power of the signal with no frequency/phase offset between the transmitters is given by,

$$P_{avg(max)|V_{o,n-TX}} = \frac{1}{2} \left(\sum_{i=1}^{n} A_i \right)^2.$$
 (17)

Here, the left inequality corresponds to the scenario when the phase offset between the i^{th} and j^{th} TX is 180° (anti-phase).

Table III summarizes the received signal power and power loss under different scenarios of frequency and phase offset between *n*-TX.

IV. FREQUENCY AND PHASE OFFSET CORRECTION

A. Frequency offset correction

Fig. 3 shows the frequency offset sensing performed at the RX. Frequency offset is detected by comparing the output voltages of open circuit rectifier using two distinct capacitors (high capacitance C_H and low capacitance C_L). The differential voltage between the rectifier consists of the ripple whose frequency is equivalent to frequency offset between the transmitters. The rectifier shown in Fig. 3 utilizes the classical Dickson multiplier topology. The open circuit rectifier has two outputs, one connected to a low capacitor (C_L <0.2pF)

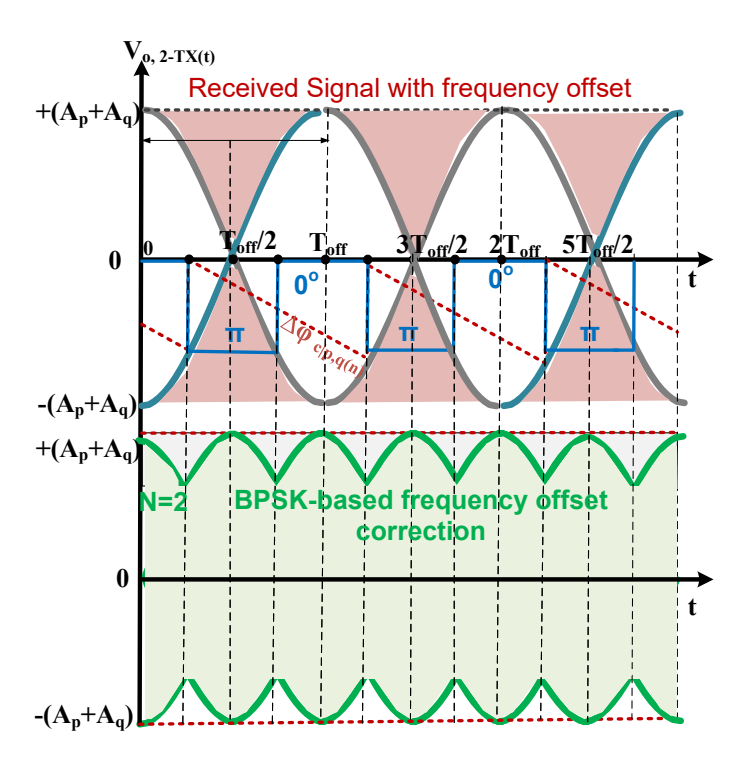


Fig. 4. PSK-based frequency correction can track the frequency offset and boost the signal power.

producing V_{FO} , while other connected to a larger capacitor $(C_H < 25 \text{pF})$ producing V_{OC} . Both outputs will settle to same DC voltage in absence of frequency offset. With frequency offset, V_{FO} will show an oscillation due to lower C_L value. V_{OC} , on the other hand, will show a much smaller ripple due to higher value of C_H . V_{OC} and V_{FO} , will be fed to an ULP comparator. Since, V_{FO} will have higher swing over V_{CO} , the comparator will generate a toggling output at Δf frequency, generating career frequency offset information. This differential voltage, which consists of frequency offset information, is encoded through the Δf sensing and the digitization block. The output is fed to a pulse generator to transmit it using backscattering. The encoded data stream is communicated to the transmitter through backscatter in the feedback loop. Once this digital stream is acquired, phase shift keying (PSK) is used to introduce dynamic phase for tracking the frequency offset. To implement frequency offset tracking, we resort to an N-point PSK-based correction scheme.

B. Analysis of frequency offset

In this analysis, we assume that the rectifier is represented by a square function followed by a low-pass filter [47]. Using (3), the output of the rectifier is given as:

$$V_{o,rect} = kx^{2} = k(A_{1}^{2} + A_{2}^{2} + 2A_{1}A_{2}cos(\Delta\alpha_{1,2}(t)) \cdot cos^{2}(\omega t + \theta)$$

$$= k(A_{1}^{2} + A_{2}^{2} + 2A_{1}A_{2}cos(\Delta\alpha_{1,2}(t)) \cdot (1 + cos(2\omega t + 2\theta)).$$
(18)

The low pass nature of the rectifier would filter high frequencies (corresponding to the carrier wave of 2ω , and we get:

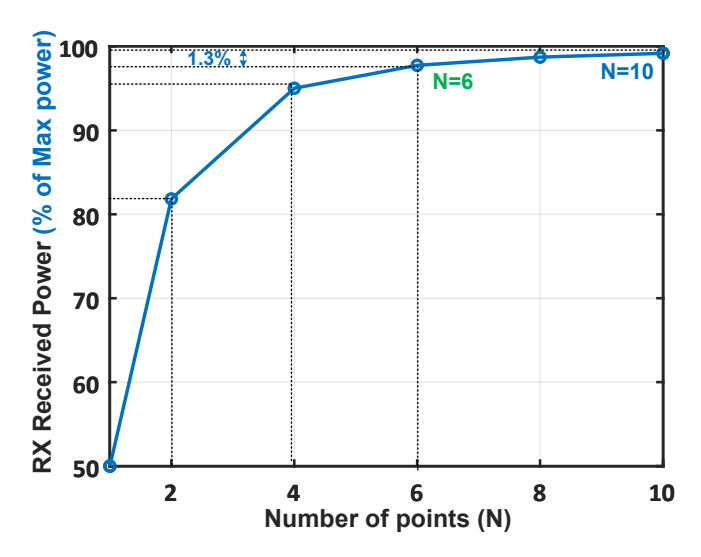


Fig. 5. Proposed PSK-based frequency offset correction scheme improves the received signal power and achieves $\approx 97\%$ of maximum power with 6-point PSK.

$$V_{o,rect} = \frac{k}{2} \left(A_1^2 + A_2^2 + 2A_1 A_2 cos(\Delta \alpha_{1,2}(t)) \right)$$

$$= \underbrace{\frac{k}{2} (A_1^2 + A_2^2)}_{PC} + k \cdot A_1 A_2 \underbrace{cos(\Delta \omega_{1,2} t + \Delta \phi_{1,2})}_{Ripple}. \quad (19)$$

Equation (19) shows that the frequency offset information is embedded in the ripple frequency of the rectifier $cos(\Delta\omega_{1,2}t)$. This modulation frequency accurately captures the frequency offset information, which is then extracted by the comparator through zero-crossings detection. Subsequently, the transmitter obtains this information using the backscatter communication. Once the transmitter acquires this information, the backscattered signal serves as the control to select from the 'N' phases and periodically phase shifts the transmitted signal. Thus, we anticipate that our method will accurately estimate the frequency offset information and transmit it to the transmitter for subsequent correction, utilizing ULP communication techniques for feedback.

Our approach to frequency correction involves addressing frequency offsets by periodically applying a specific phase shift to one of the transmitters. The magnitude of this phase shift is determined by the value of N in the N-PSK-based correction. In our BPSK-based frequency offset correction, we introduce a regular phase shift of 180° . Fig. 4 shows the BPSK for frequency offset correction. The phase shift effectively re-positions the signal, eliminating the zero-energy points observed in the received signal energy (as indicated by the zero-point crossovers in the combined signal Fig. 4).

By changing the phase of the signal at correct time instants, the envelope of signal improves, which reduces the received signal power loss (improved area under the curve in Fig. 4).

C. Optimal Condition for Frequency Correction

Equation (6) represents the mathematical basis for our PSK-based frequency offset correction technique. The essential condition to maximize power is $\Delta \alpha_{1,2}(t) = 0$, which implies

 $\beta(t) = 1$. As $\Delta \alpha_{1,2}(t)$ is a time-varying function, phase correction (static) alone would not suffice to maximize the power. To obtain the maximum possible power received frequency offset tracking and correction is needed.

This implies,

$$\underbrace{\Delta\omega_{1,2}t + \Delta\phi_{c|1,2}(t)}_{tracking} + \Delta\phi_{1,2} = 0, \tag{20}$$

where $\Delta\phi_{c|1,2}(t)$ is the frequency offset correction factor introduced to correct frequency offset by way of time varying phase. We adopt a periodic phase change approach where we introduce phase shifts with N-point phase rotation of the transmitted carrier which is at offset with the reference carrier. This method simplifies the selection of phases compared to continuous tracking. Offset correction for N-point correction is represented as,

$$\Delta \phi_{c|1,2}[n] = -\frac{\pi}{2} - \frac{\pi(2n-1)}{N}.$$
 (21)

It is essential to note that if 'T' is a very large number, the average power will asymptotically approach the integrated power over one full cycle. For instance, if 'T' is actually $'mT_{off}'$ + 't', where $'T_{off}'$ represents the frequency offset period and 'm' is a very large number, the integrated energy during 't' would be negligible compared to the total energy transferred. In such cases, the average power will approach the power transferred during one frequency offset cycle. A large integration time is often necessary for RF energy harvesting applications to harvest useful energy. Hence, we integrate over one cycle of the time period T_{off} (Fig. 4). Additionally, within the interval T_{off} , we sample the phase value at a rate of T_{off}/N . These T_{off}/N intervals are then summed to evaluate the integral with the corresponding value of $\phi[n]$ (21). By applying this correction, the envelope of the signal defined in (3) becomes:

$$V_{o,2-TX}(t) = \underbrace{\sqrt{A_1^2 + A_2^2 + 2A_1A_2cos(\Delta\alpha_{1,2}(t) + \Delta\phi_{c|1,2}[n])}} \cdot cos(\omega t + \theta).$$
New envelope
(22)

Adding the phase correction from (21) into (7), we obtain:

$$\beta(t) = \frac{1}{T_{off}} \sum_{n=1}^{N} \int_{T_1}^{T_2} \cos(\Delta \omega_{1,2} t + \Delta \phi_{1,2} + \Delta \phi_{c|1,2}[n]) dt,$$
(23)

where
$$T_1 = \frac{T_{off}}{2N} + \frac{T_{off}}{N}(n-1)$$
 and $T_2 = \frac{T_{off}}{2N} + \frac{T_{off}}{N}(n)$.

$$\beta(t) = \frac{1}{\pi} \sum_{n=1}^{N} \left(\sin\left(\frac{\pi}{N}\right) \cdot \cos\left(\Delta\phi_{1,2} - \frac{\pi(N-2)}{2N}\right) \right). \tag{24}$$

The summation term is independent of n. This implies,

$$\beta(t) = \frac{N}{\pi} sin\left(\frac{\pi}{N}\right) \cdot cos\left(\Delta\phi_{1,2} - \frac{\pi(N-2)}{2N}\right). \tag{25}$$

Equation (25) is a sinc function (sin(x)/x) where $x = \pi/N$ and approaches 1, as N approaches infinity (x goes to 0). This

implies that as N increases, the envelope of the combined signal represented by (3) becomes flatter. Substituting value of $\beta(t)$ in (6), we obtain,

$$P_{avg|V_{0,2-Tx}} = \frac{1}{2} \left(A_1^2 + A_2^2 + 2A_1 A_2 \cdot cos \left(\Delta \phi_{1,2} - \frac{\pi (N-2)}{2N} \right) \cdot \frac{N}{\pi} sin \left(\frac{\pi}{N} \right) \right). \quad (26)$$

This also confirms our earlier observation that the effect of phase offset only manifests in the combined signal power once frequency offset correction is implemented (Section III).

In Fig. 5, we present the average power of the combined signal as a function of N based on (26). The maximum power (Fig. 5 corresponds to the received signal power when there are no frequency or phase offsets between the transmitters as in Table III). With 2-point correction we boost the signal power by $\approx 80\%$, and for N=6, the combined power reaches $\approx 97\%$ and thereafter there is no significant increase in the signal power. Thus, for a practical implementation 6-point PSK is an optimal scheme for frequency offset correction. The results depicted in Fig. 5 are based on the assumption of zero-phase offset, with the intention of showcasing the maximum potential benefit of the N-PSK frequency offset correction scheme

The frequency correction algorithms, conducted using N-PSK, and its analysis reveal that while the N-PSK technique effectively corrects for frequency offset, there is a tendency to increase the value of N for achieving "near-continuous tracking." However, our analysis demonstrates that about 97% of power gets transferred at N=6.

D. Phase offset correction

Phase offset correction is implemented by sensing the rectifier voltage. The rectifier output voltage is sensed and digitized into a digital pattern using low power ADC. This encoded rectifier output voltage is received by the transmitter using the backscatter communication. The output voltage of the rectifier reaches a peak value when the phase offset between the transmitters is zero. This implies phase correction is a search algorithm, which identifies the phase offset between the transmitters and subsequently corrects it to maximize the rectifier output voltage.

The feedback mechanism for determining phase offset between the transmitters is derived from the receiver, taking into account the influence of the channel phase. Furthermore, our closed-loop technique not only considers the channel phase but also incorporates secondary effects of transmitters such as non-linearity, as well as the non-linearity of the receiver's rectifier. Since we are directly observing rectifiers output for feedback, different phase offsets because of different effects are all summed together to give the final rectifier output voltage. Eventually, phase offset because of all these effects are effectively removed then only maximum voltage will be obtained at the output of the rectifier where the harvested energy is stored. We use this output to feedback phase information. This feedback information transmitted to the transmitters is encoded digitally, ensuring its resilience to any changes in

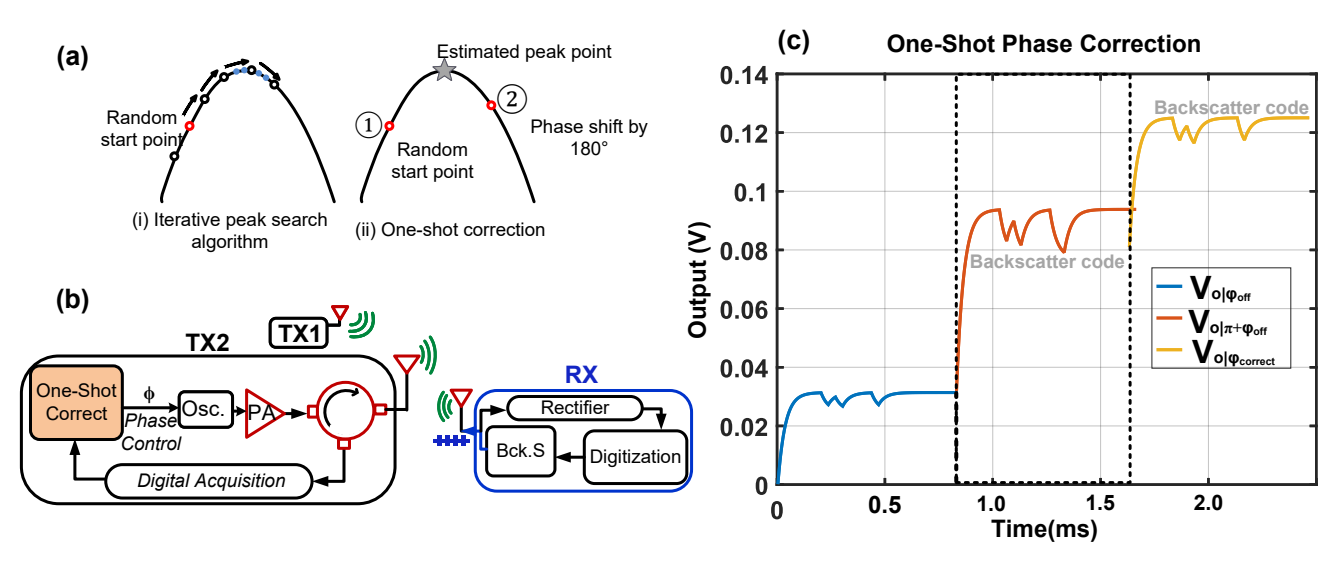


Fig. 6. (a) Proposed one-shot phase correction scheme directly settles to (or near) peak value improving convergence time, (b) System model implemented in MATLAB-Simulink with 2-TX and RX (c) Simulink simulation results for one-shot phase correction illustrates the rectifier voltage is boosted when phase offset is corrected.

channel phase and preserving the offset information intact. The correction procedure occurs at the transmitter's end, where the signal is adjusted accordingly before being transmitted through the channel.

The transmitter runs the search algorithm to process the sensed rectifier voltage. To locate the proper phase shift, which corresponds to the highest output voltage of rectifier, the transmitted signal is time delayed leading to phase shift. For maximizing received power in varying channel conditions, ϕ needs to be continuously corrected. This can be implemented by using phase varying techniques like a delay line-based phase correction technique [48]. After obtaining feedback on received power from the energy receiver, a corresponding delay to adjust LO phase is introduced using the delay-line.

E. Optimal Condition for Phase Correction

One drawback associated with a fixed-step iterative peak search algorithm is the extended convergence time it experiences as it nears the peak value (Fig. 6(a)), leading to continuous oscillation around this maximum point. Techniques like 1-bit feedback algorithm mentioned earlier address the issue of convergence at the expense of higher power consumption [29]. To optimize this, we propose a one-shot correction method to reduce the system complexity and the correction time over the conventional binary search algorithm. Fig. 6(a) shows a comparison of binary search algorithm with our proposed one-shot correction scheme. While convergence issue around the peak point is a classical problem associated with search algorithms like binary search algorithm, our proposed algorithm is one-shot by nature, and swiftly reaches the peak value or its proximity and halts, notably reducing the convergence time.

1) One-Shot Phase Correction: To analyze the one-shot correction technique, we make a mathematically simplifying assumption wherein the rectifier is assumed to be a square function followed by a low pass filter [47], In this case, the frequency offset has already been corrected, so the frequency remains the same.

$$V_{o|\phi_{off}} = kx^2 = k \left(A_1 cos(\omega t) + A_2 cos(\omega t + \phi_{off}) \right)^2. \quad (27)$$

The rectifier filters out the higher frequencies and we get,

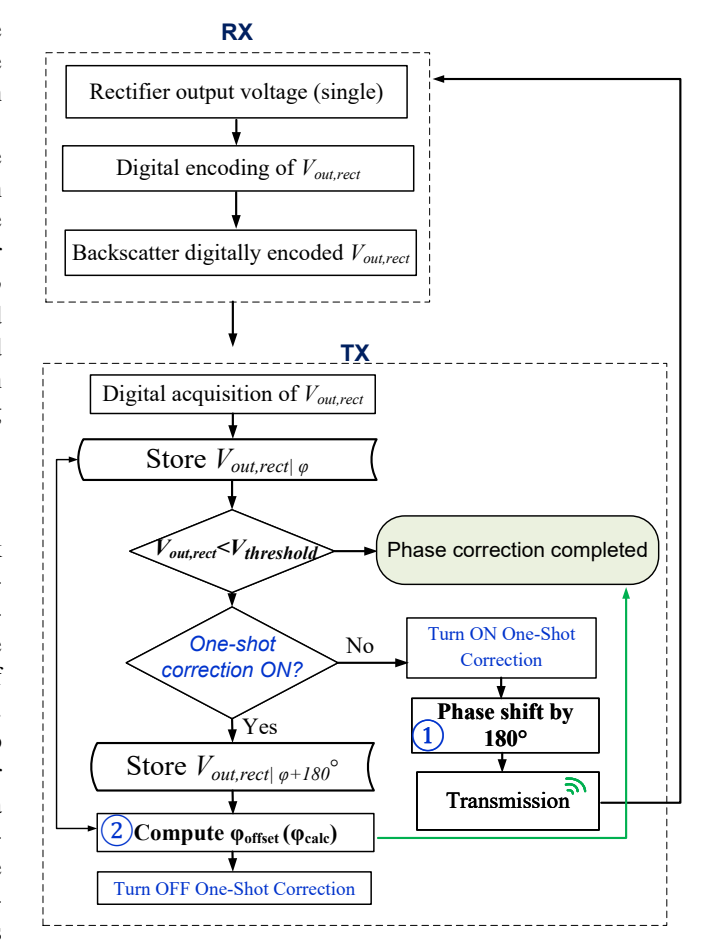


Fig. 7. Phase offset correction methodology using the proposed one-shot phase correction technique for distributed beamforming.

$$V_{o|\phi_{off}} = \frac{k}{2} (A_1^2 + A_2^2 + 2A_1 A_2 cos(\phi_{off})).$$
 (28)

We propose to shift the phase of one of the transmitters by 180° and obtain,

$$V_{o|\pi+\phi_{off}} = \frac{k}{2} (A_1^2 + A_2^2 - 2A_1 A_2 cos(\phi_{off})). \tag{29}$$

Solving (28) and (29), we see that the value of ϕ_{off} (for the case $A_1 = A_2$) is obtained as,

$$\phi_{off} = cos^{-1} \left(\frac{V_{o|\phi_{off}} - V_{o|\pi + \phi_{off}}}{V_{o|\phi_{off}} + V_{o|\pi + \phi_{off}}} \right).$$
(30)

Our method for phase offset correction relies on utilizing amplitude feedback from the received signal through backscatter communication. In instances where a phase offset exists between the transmitters, the value of the received signal at the rectifier's output is fed back to the transmitter using backscatter communication. This value is stored for subsequent computation. In the subsequent cycle, one of the transmitters alters the signal's phase by 180°. The inverse cosine of these values then reveals the original phase offset between the transmitters. Fig. 7 illustrates the pairwise implementation of our phase offset correction technique for the transmitters.

Fig. 6(b) visualizes the system model implemented in MATLAB-Simulink to verify the proposed one-shot correction technique. We have used the standard blocks (Antenna, Free Space Path Loss, amplifier, noise source, circulator, ADC, SPDT switch, variable phase block) from the RF-toolbox in Simulink to implement the system model. Fig. 6(c) presents the simulation results for the rectifier output voltage. In our simulation setup, we initialized the transmitters with a random phase offset between them. The transmitter acquired the rectifier output voltage and adjusted the signal phase by 180°. This phase adjustment was enabled by the variable phase block. The phase offset correction algorithm as depicted in Fig. 7 and based on (30), then estimates the offset between the transmitter and tunes one of the transmitter with the corrected phase. Fig. 6(c) shows that the rectifier output voltage is boosted once the phase correction is complete. The variation observed in the rectifier output voltage is on account of the interference from the backscatter code in the wireless medium. For an initial phase offset of 40° between the transmitters, the one-shot algorithm estimates the phase as 40.2°. We have simulated this for multiple phase offset points and the error between actual and estimated phase offset is $< \pm 1\%$, which shows that our technique achieves a high level of accuracy for phase correction.

V. MEASUREMENT RESULTS

Fig. 8 shows the measurement setup to demonstrate the proposed wireless distributed beamforming with frequency and phase offset correction technique. The measurements were performed in an anechoic chamber and setup comprises of wireless RF distributed beamforming from 2-TX to a receiver placed at a distance of 3.3 feet. For wireless transmission at 2.4 GHz, we used dipole antenna at both TX and RX. We have used Ettus USRP B210 SDR [49] as the transmitters and a commercial rectifier POWERCAST P21XXCSR-EVB [50] as the receiver. The measurement setup discussed in the following subsections provides details on the frequency offset and phase offset correction. The beamforming technique was first performed for 2-TX system and then extended to the 3-TX system to demonstrate its scaling to *n*-transmitter system. We also deployed a backscatter communication measurement to

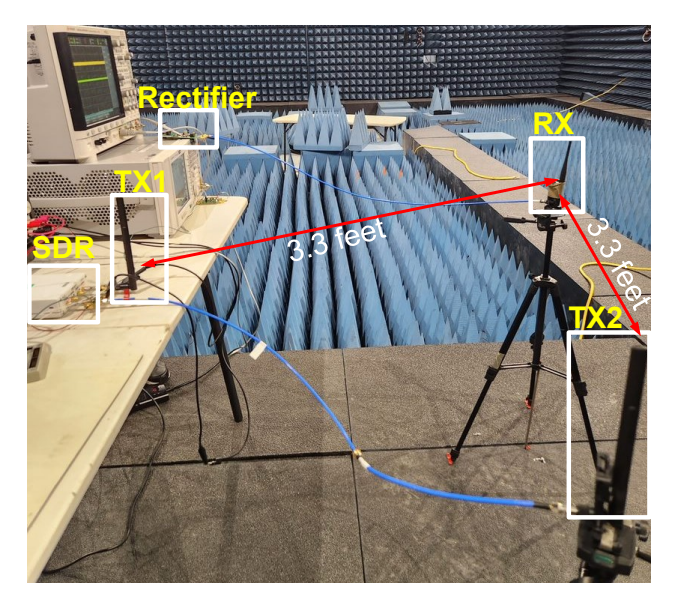


Fig. 8. Wireless RF distributed beamforming setup in the anechoic chamber with 2-TX and RX placed placed equidistant from each other.

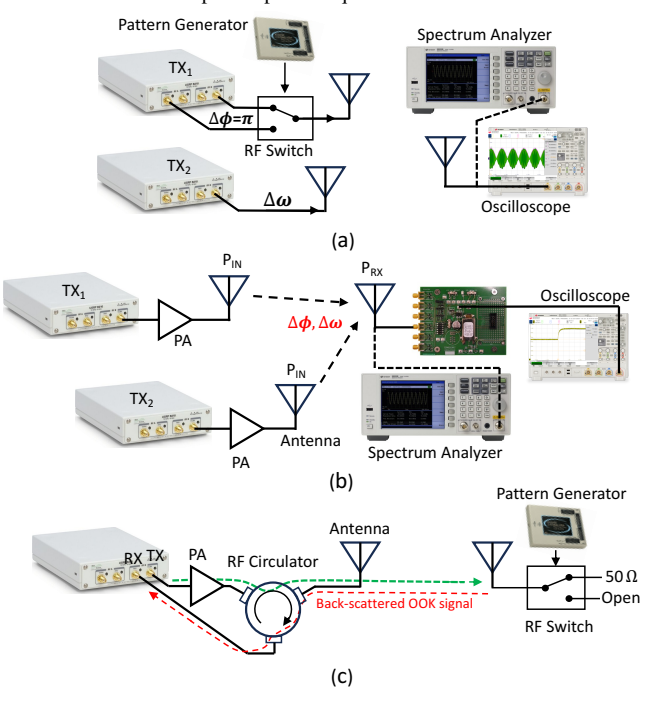


Fig. 9. Measurement setup: (a) 2-point PSK frequency offset correction; (b) phase offset correction; (c) backscatter communication based frequency/phase offset information acquisition.

develop the feedback link in the proposed system. Fig. 9 shows the specific setup for different measurements. An automation setup was developed to remotely operate the transmitters, which enabled to reduce any disturbance to the test setup during measurements.

Before conducting measurements in the anechoic chamber, we had previously assessed the rectifier's performance concerning open circuit voltage when subjected to an input RF signal, as elaborated in the following discussion.

A. Commercial Rectifier Characterization

The commercial RF energy harvester (POWERCAST P21XXCSR-EVB) consists of a passive rectifier and a boost

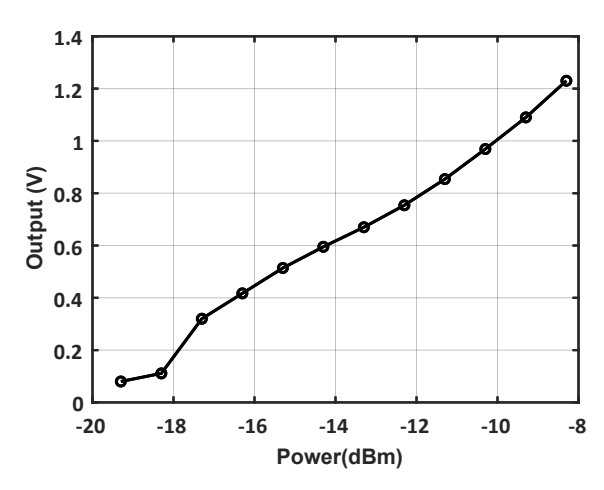


Fig. 10. Measurement result of the rectifier voltage for input RF power sweep. converter to regulate the output voltage. Fig. 10 shows the measurement results of rectifier open circuit output voltage for the input RF signal power sweep. The rectifier presents a linear characteristics from -17 dBm to -8 dBm range. For higher RF power, boost converter regulates the output voltage. In our setup, we calibrated the trigger of boost converter such that the output voltage is regulated at 1.2V for higher signal power (above -8 dBm). The rectifier characterization serves as a look up table for our measurement setup to assess the received signal strength and calibrate TXs power.

B. Path Loss Characterization

Fig. 8 shows the wireless measurement setup with a 3.3 feet distance between each TX and RX. Each TX sends a continuous wave (CW) RF power at 2.4 GHz frequency. To maximize the transmitting power, we used a power amplifier (PMA4-33GLN+) at the SDR output port. Considering the signal amplification and accounting for losses incurred through cable and antenna, we transmit an effective power of +25 dBm from TX1 and TX2. For a distance of 3.3 feet, we observe on spectrum analyzer (KEYSIGHT N9010A) a received signal of -16 dBm. This indicates an effective path loss of 41 dB (40.5 dB theoretical free space path loss at 2.4 GHz).

C. Frequency Offset Correction

Fig. 9 (a) shows the setup for our 2-point-based frequency offset correction. We performed our experiments by setting a 10 kHz offset between the two transmitters, which corresponds to approximately 4.2 parts-per-million (ppm) offset at 2.4 GHz. We introduced this 10 KHz frequency offset between the transmitters by calibrating the carrier frequency of each SDR programmed using GNU Radio.

As detailed in Section II-A, the suggested frequency correction method employs PSK-based correction. This correction is achieved by periodically introducing a 180° phase offset between two output ports of TX1, mimicking the behavior of a BPSK modulated signal from TX1.

This implementation utilizes an RF switch (HSWA2-30DR+[51]), controlled by a pattern generator (IO-3200), to regulate the "symbol rate" of the BPSK-like signal. In our arrangement,

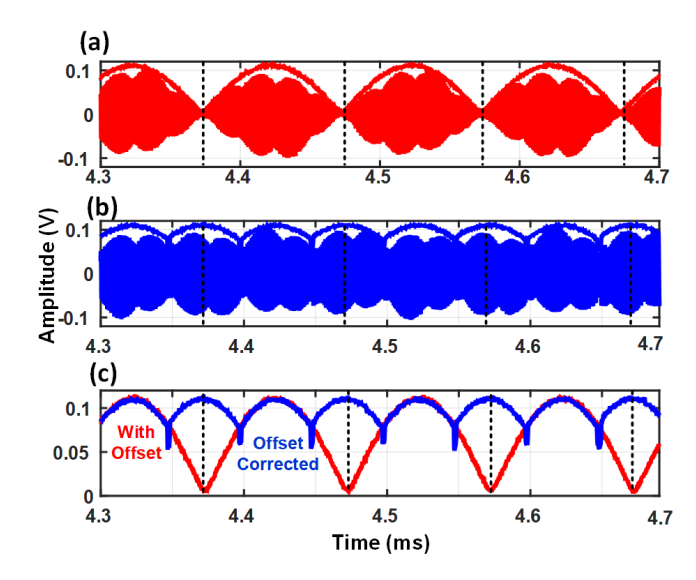


Fig. 11. Measurement results: (a) combined RF signal with 10 kHz frequency offset between TX1 and TX2; (b) combined RF signal after frequency offset correction; (c) combined RF signal envelope comparison between before and after frequency offset correction.

the RF1 and RF2 inputs to the RF switch were generated from the SDR, exhibiting a 180° phase difference between them. The generation of CONTROL1 signal (CONTROL2 is set to '0') was implemented by the pattern generator (IO3200). It is critical to introduce the BPSK modulated signal at the right time instant (Fig. 4). To achieve this time synchronization, we implemented a controlled delay in the control signal from the pattern generator

Fig. 11(a) demonstrates the received RF signal waveform with 10 KHz frequency offset observed on the oscilloscope (KEYSIGHT MSOX6004A). Fig. 11(b) presents the RF signal voltage after 2-point frequency correction. This matches with our analysis presented in Fig. 4. Fig. 11 shows the envelope of the received signal before and after frequency offset correction. The frequency offset correction boosts the signal strength, evident from the envelope of the received signal. flatter the envelope means better correction In our 2point correction measurement, we observe output power is 79.7% of the maximum possible received signal power. This closely matches with the theoretical value of 81.8% from our analysis (Fig. 5). This validates the accuracy of the frequency correction in enhancing the receiver signal power. BPSK-based frequency offset correction results in an additional 2 dB gain in the received signal strength. As additional correction points are utilized (N = 6, as the optimal condition), the envelope of received signal gradually approaches a constant envelope, eliminating any remaining frequency offset and boosting signal strength.

D. Phase offset and correction

Fig. 9(b) shows the setup for phase offset correction between the transmitters. We observe the rectifier's output voltage to quantify the effect of phase offset between the transmitters. Each TX transmits a power of +25 dBm. An oscilloscope is connected to PC to save the output voltage of the rectifier corresponding to each phase offset. The automation

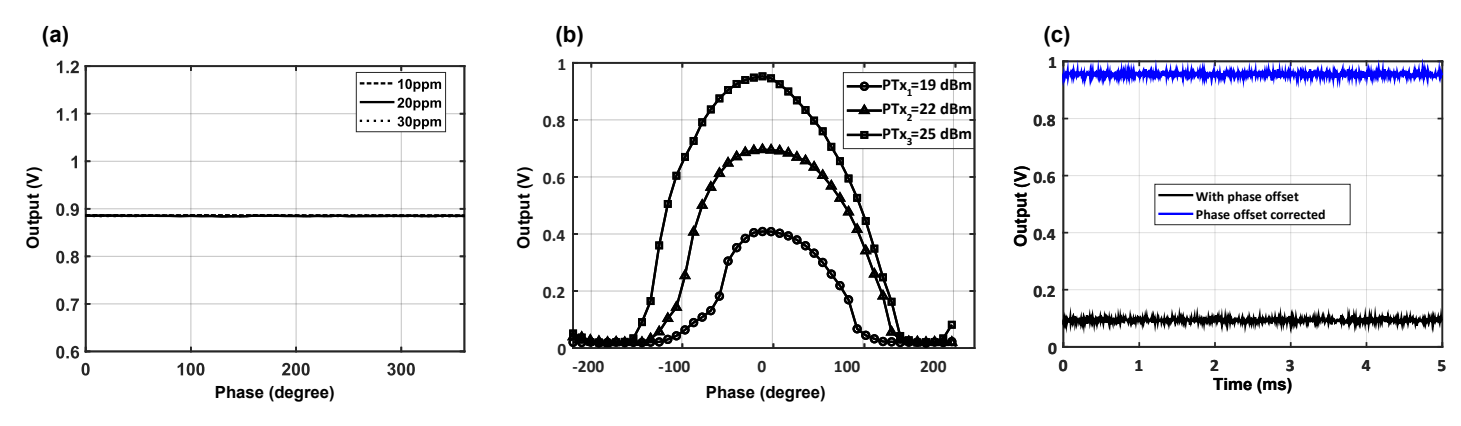


Fig. 12. (a) Measured rectifier voltage is invariant to phase changes if a frequency offset exists between transmitters, (b) Measured rectifier voltage with phase sweep (zero frequency offset) for different power, (c) Rectifier voltage is boosted when phase offset between transmitters is corrected.

setup is used to sweep the phase offset and record rectifier output voltage.

To confirm our analysis indicating the necessity of correcting frequency offset before addressing phase offset, we execute a phase sweep between the two transmitters for different frequency offsets in the SDR programmed using GNU radio. Fig. 12(a) shows the measurement results for the rectifier output voltage with phase sweep done at different frequency offset. We note that in the presence of a frequency offset between the transmitters, the rectifier output remains consistent for a given RF power level. This shows that correcting any phase offset between transmitters proves ineffective in maximizing signal power unless the frequency offset is corrected beforehand.

We then calibrated the carrier frequency of each TX from GNU radio, so that there is no frequency offset between the transmitters. Fig. 12(b) presents the measurement results of the rectifier output voltage when we vary the phase between the transmitter with zero frequency offset. We observe that the rectifier output reaches a maximum value when the phase difference between the transmitters is zero (9). Fig. 12(c) shows the rectifier output voltage with time when we have a random phase offset between the transmitters. This corresponds to a near-zero rectifier output voltage. When we correct for the phase, we observe the rectifier output voltage is boosted up to 1V. This corresponds to –10 dBm of received power (Fig. 10), which is a +6 dB gain in the signal strength (–16 dBm from each TX after path loss) obtained from phase and frequency offset correction.

1) 1-shot phase correction: We also validate the accuracy of our one-shot phase correction algorithm outlined in Section IV-E to estimate and correct phase offset between the transmitters. For each value of phase offset between the transmitters, we estimate the phase offset from (30), where the rectifier voltage for a given phase offset is obtained from Fig. 12(b). In Fig. 13, we present the phase offset estimated from our proposed one-shot phase correction algorithm. Our proposed one-shot phase correction algorithm is able to accurately predict the phase offset between the transmitters with maximum error of ±5%.

E. Backscatter Communication

Backscatter communication is critical in our setup as it is the feedback link to obtain the frequency and phase offset

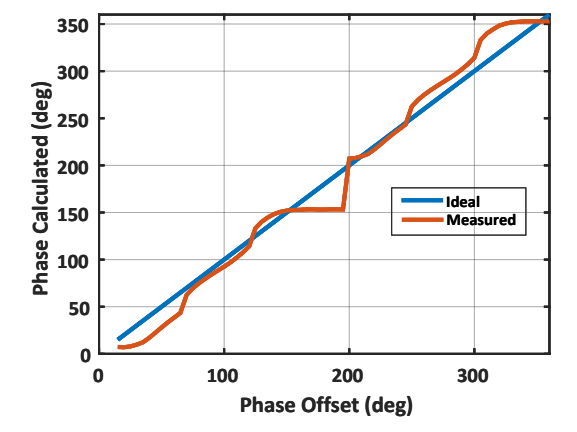


Fig. 13. The measured accuracy of one-shot phase correction technique.

information from the receiver. In our measurement, we verified the feasibility of using backscatter technique to transmit encoded pattern back to transmitter. Fig. 9(c) shows the measurement setup for backscatter communication. We transmit a CW signal of +25 dBm from the transmitter. We generate an OOK modulated pattern using an RF switch (HSWA2-30DR+) controlled by pattern generator (IO-3200) to reflect OOK modulated signal to the receiver. SDR is configured as a full-duplex transceiver by deploying an RF circulator (PE83CR1030 [52]) to isolate TX-RX path for simultaneous signal transmission and reception. The backscattered signal is received by the TX after it encounters a two-way path loss of 82 dB. The estimated received backscattered signal strength is around -57 dBm. Additionally, the limited isolation of RF circulator adds to the noise floor of the receiver degrading the signal to noise ratio (SNR). To address this in our measurement setup, we improved the RF isolation of the circulator from 25 dB to 40 dB by cascading two RF circulators. This results in an improvement in the SNR. Fig. 14 shows the results of the received backscattered signal after demodulation from the SDR. The received pattern matches with the transmitted pattern from the RX. Further an ULP RSSI circuit, which can filter out CW signal at 6 nW power can further improve the SNR [40].

F. n-Transmitter Beamforming

From our previous measurement results, we obtain $\approx +6$ dB gain in signal strength from 2-TX. To demonstrate the wireless beamforming with n additional transmitters, we introduced a third transmitter in our setup. Similar to our measurement

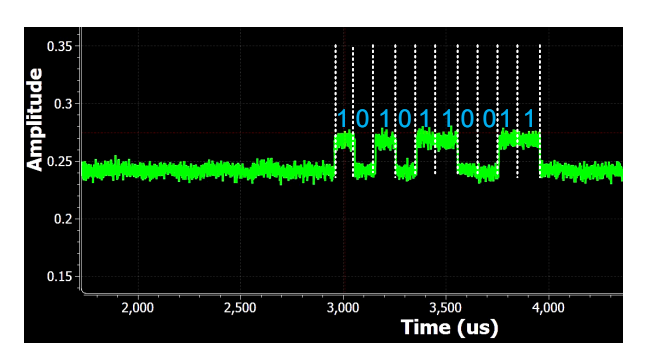


Fig. 14. Acquired digital code at the TX using backscatter communication.

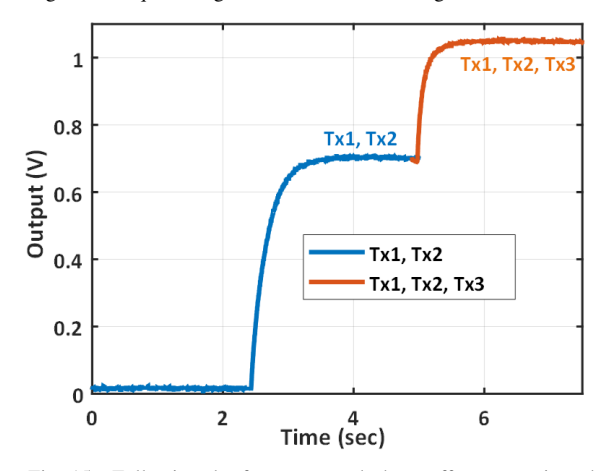


Fig. 15. Following the frequency and phase offset correction, the rectifier's output voltage experiences an increase upon the introduction of a third transmitter.

setup with 2-TX system, we positioned the third transmitter at a distance of 3.3 feet from the RX. We calibrated the transmitters such that there is no frequency offset between the transmitters. Each transmitter transmits an effective power of +23 dBm (-18 dBm received at the RX after 41 dB of path loss). We correct the phase offset between the transmitters in a pairwise manner, and this approach is deemed suitable for *n*-TX [53]. Fig. 15 shows the rectifier output voltage from multiple transmitters. First, we correct the phase offset between TX1 and TX2 and then between TX1 (or TX2) and TX3. Finally, rectifier output voltage settles to a voltage of 1.2V as seen in Fig. 15. This corresponds to an equivalent received signal power of -8.5 dBm incident power read from Fig. 10 and the total power gain is 9.5 dB (9X) from 3-TX.

Measurement results shows the received signal strength obtained from wireless beamforming with both the 2-TX and 3-TX configurations, demonstrating consistent agreement with the results detailed in Table III. We extrapolate that deploying n-transmitters for wireless distributed beamforming, post pairwise correction for frequency and phase offsets, anticipates a signal strength enhancement by a factor of n^2 compared to individual received power. This proposed optimal distributed beamforming strategy, combined with an efficient RF-to-DC harvester, establishes a wireless power transfer system tailored for ULP IoT systems. Fig. 16 illustrates the relative gain resulting from frequency and phase offset correction as the number of transmitters increases. With an increasing number of transmitters, the transmitted power from each TX decreases

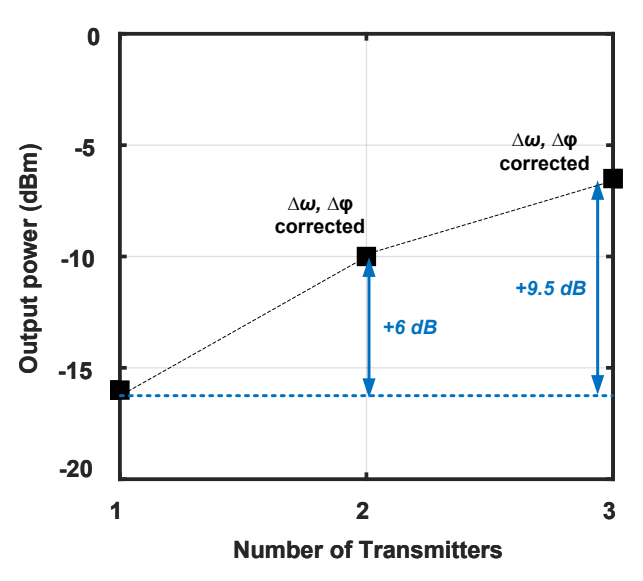


Fig. 16. Relative gain in the received signal power with number of transmitters.

to maintain a given signal power at the RX, leading to enhanced energy efficiency of the TX. Additionally, with constant TX power, the harvested power at the RX increases, further improving the efficiency of the rectifier [54]. We have validated our analysis and algorithm for offset correction through successful validation of a multi-transmitter to single receiver (MISO) system. We expect that this system can be extended to include multiple energy receivers which will involve pairwise correction for transmitters for each given receiver. Such capability can be included as new features into MAC layer of network protocols [55].

Table IV compares our approach with existing methods in wireless power transfer. In [56], [58], [59], an external clock synchronizes the frequency between transmitters by distributing a common clock to overcome frequency offset issue. However, in real applications LOs cannot be shared and would remain distributed with in-built frequency offsets even in same channel. [57] explores Extended Kalman Filter (EKF) for frequency offset correction. Other approaches have used GPS disciplined oscillator (GPSDO) with oven-compensated XO (OCXO) [60], [61] to have same LO for transmitters. However, having OCXOs and GPS clocks would incur power overhead in watts [62], [63] with additional size overhead of GPS antenna.

For phase offset correction, [56], [57] implement CSI feedback processed at the TX. [59] employs a blind adaptive beamforming algorithm on commercial Software Defined Radio (SDR) for phase offset correction. [56] achieves a beamforming gain of 11.67 dB for 4-TX and 6.87 dB for 3-TX systems. [59] achieves a power gain of < 6 dB for a 4-TX system, whereas our closed-loop beamforming attains a 9.5 dB gain for a 3-TX setup using backscatter communication for offset feedback. For phase offset feedback, [57], [58] embed offset information using the radio at the RX to communicate with the TX, while [59] directly connects to a PC and processes phase offset using Python. Compared to [57]–[59], our approach introduces an energy-efficient phase and frequency offset sensing and correction scheme for the receiver

TABLE IV

COMPARISON OF THIS WORK WITH OTHER REPORTED WORKS ON WPT.

Parameters	IMWUT '23 [56]	IEEE ToN '21 [57]	Wirel. Commun. '17 [58]	IEEE Access '17 [59]	Our work
WPT range (m)	> 3.5	1	< 5	< 1.5	1
TX power (dBm)	24	34.77 (3W)	21.6 (≈145mW)	20	23
Antenna gain (dBi)	12	3.98	N/A	8	0
TX Carrier frequency	900 MHz	2.4 GHz	920 MHz	915 MHz	2.4 GHz
LO sync.	CDA-2990	EKF	OctoClock	NI Octoclock-G	NPSK
Freq. correction accuracy	Locked ext.	N/A	Locked ext.	Locked ext.	97% ¹
Phase corr. method	CSI	One-bit feedback	Linear estimation	Blind-adaptive	One-Shot correction
Phase corr. error	Not specified	N/A	0.01 mW ²	0.1%	± 5%
Freq./Phase offset feedback	Backscatter	Ettus B210	Zolertia Z1	Direct PC	Backscatter
Offset sensing power	Not specified	Ettus B210 (radio)	Zolertia Z1 (radio)	Software	< 30 nW ³
Max. number of TX	4	4	6	4	3
Max. RX Power Gain (dB)	11.76 6.87 (3-TX)	Not specified	≈ 5	< 6	9.5

¹ Max. with 6-PSK, ² Std deviation, ³ Estimated based on simulation and measurement of 65-nm CMOS circuits.

using backscatter communication. Our proposed beamforming infrastructure consumes power (nWs) that is orders of magnitude lower than systems using conventional radios (mWs) to transmit offset feedback information. This allows the receiver to operate with ultra-low power consumption, benefiting from ultra-low power distributed beamforming.

VI. CONCLUSIONS

In this paper, we introduced an efficient distributed beamforming system designed for RF energy harvesting from multiple transmitters to an IoT device. We presented design analysis to quantify the power loss in the combined signal received due to frequency and phase offsets among the transmitters. Our analysis reveals that upon correcting these frequency and phase discrepancies among the transmitters, there is potential to amplify the combined signal power by a factor of n^2 in scenarios involving n-transmitters within the distributed beamforming network. The analysis offers insights for establishing a method to correct phase and frequency offsets. Moreover, we outlined optimal conditions to expedite this correction process. Our proposed framework obtains information on frequency and phase offsets from the IoT receiver using backscatter communication, enabling a highly efficient sensing system with ultra-low power consumption. Following this, we verified the efficacy of our proposed frequency and phase correction methodology by conducting experiments in an anechoic chamber, initially involving two transmitters and subsequently three transmitters along with a receiver. These experiments showed the reliability of backscatter communication as a viable method for optimizing distributed beamforming, all while ensuring ultra-low power consumption.

VII. ACKNOWLEDGEMENTS

The authors thank Max Turkewitz from Northeastern KRI facility of Burlington, MA, for his help with the measurement setup in the anechoic chamber and Hao Zuo, Handan Gu for their help to facilitate the measurement in Burlington.

REFERENCES

[1] "IoT market size worldwide 2017-2025." [Online]. Available: https://www.statista.com/statistics/976313/global-iot-market-size/

- [2] X. Zhang, J. Grajal, M. López-Vallejo, E. McVay, and T. Palacios, "Opportunities and Challenges of Ambient Radio-Frequency Energy Harvesting," *Joule*, vol. 4, no. 6, pp. 1148–1152, 2020. [Online]. Available: https://www.sciencedirect.com/science/article/pii/S2542435120301896
- [3] B. Clerckx, R. Zhang, R. Schober, D. W. K. Ng, D. I. Kim, and H. V. Poor, "Fundamentals of Wireless Information and Power Transfer: From RF Energy Harvester Models to Signal and System Designs," *IEEE Journal on Selected Areas in Communications*, vol. 37, no. 1, pp. 4–33, 2019.
- [4] K. W. Choi, S. I. Hwang, A. A. Aziz, H. H. Jang, J. S. Kim, D. S. Kang, and D. I. Kim, "Simultaneous Wireless Information and Power Transfer (SWIPT) for Internet of Things: Novel Receiver Design and Experimental Validation," *IEEE Internet of Things Journal*, vol. 7, no. 4, pp. 2996–3012, 2020.
- [5] D. Mishra, S. De, and D. Krishnaswamy, "Dilemma at RF Energy Harvesting Relay: Downlink Energy Relaying or Uplink Information Transfer?" *IEEE Transactions on Wireless Communications*, vol. 16, no. 8, pp. 4939–4955, 2017.
- [6] U. Muncuk, K. Alemdar, J. D. Sarode, and K. R. Chowdhury, "Multi-band Ambient RF Energy Harvesting Circuit Design for Enabling Batteryless Sensors and IoT," *IEEE Internet of Things Journal*, vol. 5, no. 4, pp. 2700–2714, 2018.
- [7] M. Piñuela, P. D. Mitcheson, and S. Lucyszyn, "Ambient RF Energy Harvesting in Urban and Semi-Urban Environments," *IEEE Transactions* on Microwave Theory and Techniques, vol. 61, no. 7, pp. 2715–2726, 2013.
- [8] P. Xu, D. Flandre, and D. Bol, "A Self-Gating RF Energy Harvester for Wireless Power Transfer With High-PAPR Incident Waveform," *IEEE Journal of Solid-State Circuits*, vol. 56, no. 6, pp. 1816–1826, 2021.
- [9] J. Yi, W.-H. Ki, and C.-Y. Tsui, "Analysis and Design Strategy of UHF Micro-Power CMOS Rectifiers for Micro-Sensor and RFID Applications," *IEEE Transactions on Circuits and Systems I: Regular Papers*, vol. 54, no. 1, pp. 153–166, 2007.
- [10] M. A. Abouzied, K. Ravichandran, and E. Sánchez-Sinencio, "A Fully Integrated Reconfigurable Self-Startup RF Energy-Harvesting System With Storage Capability," *IEEE Journal of Solid-State Circuits*, vol. 52, no. 3, pp. 704–719, 2017.
- [11] P. Saffari, A. Basaligheh, and K. Moez, "An RF-to-DC Rectifier With High Efficiency Over Wide Input Power Range for RF Energy Harvesting Applications," *IEEE Transactions on Circuits and Systems I: Regular Papers*, vol. 66, no. 12, pp. 4862–4875, 2019.
- [12] M. Wagih, G. S. Hilton, A. S. Weddell, and S. Beeby, "Millimeter-Wave Power Transmission for Compact and Large-Area Wearable IoT Devices Based on a Higher Order Mode Wearable Antenna," *IEEE Internet of Things Journal*, vol. 9, no. 7, pp. 5229–5239, 2022.
- [13] Z. He and C. Liu, "A Compact High-Efficiency Broadband Rectifier With a Wide Dynamic Range of Input Power for Energy Harvesting," *IEEE Microwave and Wireless Components Letters*, vol. 30, no. 4, pp. 433–436, 2020.
- [14] M.-Y. Huang, T. Chi, F. Wang, and H. Wang, "An All-Passive Negative Feedback Network for Broadband and Wide Field-of-View Self-Steering Beam-Forming With Zero DC Power Consumption," *IEEE Journal of Solid-State Circuits*, vol. 52, no. 5, pp. 1260–1273, 2017.

- [15] V. Kuhn, C. Lahuec, F. Seguin, and C. Person, "A Multi-Band Stacked RF Energy Harvester With RF-to-DC Efficiency Up to 84%," *IEEE Transactions on Microwave Theory and Techniques*, vol. 63, no. 5, pp. 1768–1778, 2015.
- [16] B. Li, X. Shao, N. Shahshahan, N. Goldsman, T. Salter, and G. M. Metze, "An Antenna Co-Design Dual Band RF Energy Harvester," *IEEE Transactions on Circuits and Systems I: Regular Papers*, vol. 60, no. 12, pp. 3256–3266, 2013.
- [17] L. Guo, X. Li, P. Chu, and K. Wu, "Accurately Modeling Zero-Bias Diode-Based RF Power Harvesters With Wide Adaptability to Frequency and Power," *IEEE Transactions on Circuits and Systems I: Regular Papers*, vol. 68, no. 12, pp. 5194–5205, 2021.
- [18] O. L. A. López, B. Clerckx, and M. Latva-Aho, "Dynamic RF Combining for Multi-Antenna Ambient Energy Harvesting," *IEEE Wireless Communications Letters*, vol. 11, no. 3, pp. 493–497, 2022.
- [19] D.-J. Lee, S.-J. Lee, I.-J. Hwang, W.-S. Lee, and J.-W. Yu, "Hybrid Power Combining Rectenna Array for Wide Incident Angle Coverage in RF Energy Transfer," *IEEE Transactions on Microwave Theory and Techniques*, vol. 65, no. 9, pp. 3409–3418, 2017.
- [20] Z. Liu, P. Wu, and G. Li, "A Multibeam and Surface Plasmonic Clothing With RF Energy-Localized Harvester for Powering Battery-Free Wireless Sensor," *IEEE Internet of Things Journal*, vol. 9, no. 15, pp. 13 955–13 964, 2022.
- [21] S. Kim, H.-W. Jo, J.-W. Kim, J.-I. Oh, J.-W. Yu, and B. Ahn, "Curved-Retrodirective Beamforming System to Improve Microwave Power Transmission Efficiency in the Fresnel Region," *IEEE Internet of Things Journal*, vol. 10, no. 17, pp. 15012–15024, 2023.
- [22] J. Liu, M. Huang, Y. Lu, and R. P. Martins, "RF Rectifiers With Wide Incident Angle of Incoming Waves Based on Rat-Race Couplers," *IEEE Transactions on Microwave Theory and Techniques*, vol. 70, no. 3, pp. 1983–1993, 2022.
- [23] W. M. Abdulkawi, M. A. Alqaisei, A.-F. A. Sheta, and I. Elshafiey, "New Compact Antenna Array for MIMO Internet of Things Applications," *Micromachines*, vol. 13, no. 9, p. 1481, 2022.
- [24] L. Lizzi, F. Ferrero, P. Monin, C. Danchesi, and S. Boudaud, "Design of miniature antennas for IoT applications," in 2016 IEEE Sixth International Conference on Communications and Electronics (ICCE), 2016, pp. 234–237.
- [25] R. Mudumbai, D. R. Brown Iii, U. Madhow, and H. V. Poor, "Distributed transmit beamforming: challenges and recent progress," *IEEE Communications Magazine*, vol. 47, no. 2, pp. 102–110, 2009.
- [26] E. Sourour, H. El-Ghoroury, and D. McNeill, "Frequency offset estimation and correction in the ieee 802.11a wlan," in *IEEE 60th Vehicular Technology Conference*, 2004. VTC2004-Fall. 2004, vol. 7, 2004, pp. 4923–4927 Vol. 7.
- [27] M. Seo, M. Rodwell, and U. Madhow, "A feedback-based distributed phased array technique and its application to 60-GHz wireless sensor network," in 2008 IEEE MTT-S International Microwave Symposium Digest, 2008, pp. 683–686.
- [28] S. Sharma and S. De, "Distributed RF Beamforming for Wireless Power Transfer Over Time Varying Channels," in ICC 2023 - IEEE International Conference on Communications, 2023, pp. 919–924.
- [29] R. Mudumbai, J. Hespanha, U. Madhow, and G. Barriac, "Distributed Transmit Beamforming Using Feedback Control," *IEEE Transactions on Information Theory*, vol. 56, no. 1, pp. 411–426, 2010.
- [30] W.-Q. Wang, "Carrier Frequency Synchronization in Distributed Wireless Sensor Networks," *IEEE Systems Journal*, vol. 9, no. 3, pp. 703–713, 2015
- [31] S. R. Mghabghab and J. A. Nanzer, "Open-Loop Distributed Beamforming Using Wireless Frequency Synchronization," *IEEE Transactions on Microwave Theory and Techniques*, vol. 69, no. 1, pp. 896–905, 2021.
- [32] Z. Xu, A. Khalifa, A. Mittal, M. Nasrollahpourmotlaghzanjani, D. Das, M. Onabajo, N. X. Sun, S. S. Cash, and A. Shrivastava, "A 30% Efficient High-Output Voltage Fully Integrated Self-Biased Gate RF Rectifier Topology for Neural Implants," *IEEE Journal of Solid-State Circuits*, vol. 57, no. 11, pp. 3324–3335, 2022.
- [33] V. Liu, A. Parks, V. Talla, S. Gollakota, D. Wetherall, and J. R. Smith, "Ambient Backscatter: Wireless Communication out of Thin Air," in *Proceedings of the ACM SIGCOMM 2013 Conference on SIGCOMM*, ser. SIGCOMM '13. New York, NY, USA: Association for Computing Machinery, 2013, p. 39–50. [Online]. Available: https://doi.org/10.1145/2486001.2486015
- [34] B. Kellogg, V. Talla, S. Gollakota, and J. R. Smith, "Passive Wi-Fi: Bringing Low Power to Wi-Fi Transmissions," in 13th USENIX Symposium on Networked Systems Design and Implementation (NSDI 16). Santa Clara, CA: USENIX Association, Mar. 2016,

- pp. 151–164. [Online]. Available: https://www.usenix.org/conference/nsdi16/technical-sessions/presentation/kellogg
- [35] P.-H. P. Wang, C. Zhang, H. Yang, M. Dunna, D. Bharadia, and P. P. Mercier, "A Low-Power Backscatter Modulation System Communicating Across Tens of Meters With Standards-Compliant Wi-Fi Transceivers," *IEEE Journal of Solid-State Circuits*, vol. 55, no. 11, pp. 2959–2969, 2020.
- [36] S. J. Thomas, E. Wheeler, J. Teizer, and M. S. Reynolds, "Quadrature Amplitude Modulated Backscatter in Passive and Semipassive UHF RFID Systems," *IEEE Transactions on Microwave Theory and Techniques*, vol. 60, no. 4, pp. 1175–1182, 2012.
- [37] A. Shirane, Y. Fang, H. Tan, T. Ibe, H. Ito, N. Ishihara, and K. Masu, "RF-Powered Transceiver With an Energy- and Spectral-Efficient IF-Based Quadrature Backscattering Transmitter," *IEEE Journal of Solid-State Circuits*, vol. 50, no. 12, pp. 2975–2987, 2015.
- [38] D. Bharadia, K. R. Joshi, M. Kotaru, and S. Katti, "BackFi: High Throughput WiFi Backscatter," SIGCOMM Comput. Commun. Rev., vol. 45, no. 4, p. 283–296, aug 2015. [Online]. Available: https://doi.org/10.1145/2829988.2787490
- [39] A. Mittal and A. Shrivastava, "Detecting Continuous Jamming Attack using Ultra-low Power RSSI Circuit," in 2022 IEEE International Symposium on Hardware Oriented Security and Trust (HOST), 2022, pp. 49–52.
- [40] A. Mittal, N. Mirchandani, G. Michetti, L. Colombo, T. Haque, M. Rinaldi, and A. Shrivastava, "A ±0.5 dB, 6 nW RSSI Circuit With RF Power-to-Digital Conversion Technique for Ultra-Low Power IoT Radio Applications," *IEEE Transactions on Circuits and Systems I: Regular Papers*, vol. 69, no. 9, pp. 3526–3539, 2022.
- [41] A. Wang, C. Chen, and C. R. Shi, "Design and Analysis of an Always-ON Input-Biased pA-Current Sub-nW mV-Threshold Hysteretic Comparator for Near-Zero Energy Sensing," *IEEE Transactions on Circuits* and Systems 1: Regular Papers, vol. 64, no. 9, pp. 2284–2294, 2017.
- [42] Z. Zhu and Y. Liang, "A 0.6-V 38-nW 9.4-ENOB 20-kS/s SAR ADC in 0.18-\(\mu\mathrm{m}\) CMOS for Medical Implant Devices," *IEEE Transactions on Circuits and Systems I: Regular Papers*, vol. 62, no. 9, pp. 2167–2176, 2015.
- [43] W. Hu, Y.-T. Liu, T. Nguyen, D. C. Lie, and B. P. Ginsburg, "An 8-Bit Single-Ended Ultra-Low-Power SAR ADC With a Novel DAC Switching Method and a Counter-Based Digital Control Circuitry," *IEEE Transactions on Circuits and Systems I: Regular Papers*, vol. 60, no. 7, pp. 1726–1739, 2013.
- [44] P. Harpe, H. Gao, R. v. Dommele, E. Cantatore, and A. H. M. van Roermund, "A 0.20 mm² 3 nW Signal Acquisition IC for Miniature Sensor Nodes in 65 nm CMOS," *IEEE Journal of Solid-State Circuits*, vol. 51, no. 1, pp. 240–248, 2016.
- [45] J. Yi, W.-H. Ki, and C.-Y. Tsui, "Analysis and Design Strategy of UHF Micro-Power CMOS Rectifiers for Micro-Sensor and RFID Applications," *IEEE Transactions on Circuits and Systems I: Regular Papers*, vol. 54, no. 1, pp. 153–166, 2007.
- [46] G. Papotto, F. Carrara, and G. Palmisano, "A 90-nm CMOS Threshold-Compensated RF Energy Harvester," *IEEE Journal of Solid-State Circuits*, vol. 46, no. 9, pp. 1985–1997, 2011.
- [47] N. Mirchandani, Y. Zhang, S. Abdelfattah, M. Onabajo, and A. Shrivastava, "Modeling and Simulation of Circuit-Level Nonidealities for an Analog Computing Design Approach With Application to EEG Feature Extraction," *IEEE Transactions on Computer-Aided Design of Integrated Circuits and Systems*, vol. 42, no. 1, pp. 229–242, 2023.
- [48] P. A. J. Nuyts, P. Singerl, F. Dielacher, P. Reynaert, and W. Dehaene, "A fully digital delay line based ghz range multimode transmitter front-end in 65-nm cmos," *IEEE Journal of Solid-State Circuits*, vol. 47, no. 7, pp. 1681–1692, 2012.
- [49] "USRP B210 USB Software Defined Radio (SDR)." [Online]. Available: https://www.ettus.com/all-products/ub210-kit/
- [50] Powercast, "P21XXCSR-EVB," Datasheet, 2018. [Online]. Available: https://www.mouser.com/datasheet/2/329/P21XXCSR_EVB_Datasheet_v2_1_1-3159484.pdf
- [51] Mini-Circuits, HSWA2-30DR+ SPDT RF SWITCH, Online. [Online]. Available: https://www.minicircuits.com/pdfs/HSWA2-30DR+.pdf
- [52] Pasternack, "Circulators Technical Datasheet PE83CR1030," Datasheet, 2018. [Online]. Available: https://www.pasternack.com/images/ProductPDF/PE83CR1030.pdf
- [53] F. Quitin, U. Madhow, M. M. U. Rahman, and R. Mudumbai, "Demonstrating distributed transmit beamforming with software-defined radios," in 2012 IEEE International Symposium on a World of Wireless, Mobile and Multimedia Networks (WoWMoM), 2012, pp. 1–3.
- [54] Z. Xu, A. Khalifa, A. Mittal, M. Nasrollahpourmotlaghzanjani, R. Etienne-Cummings, N. Xiang Sun, S. S. Cash, and A. Shrivastava,

- "Analysis and Design Methodology of RF Energy Harvesting Rectifier Circuit for Ultra-Low Power Applications," *IEEE Open Journal of Circuits and Systems*, vol. 3, pp. 82–96, 2022.
 [55] S. Mohanti, E. Bozkaya, M. Y. Naderi, B. Canberk, G. Secinti, and
- [55] S. Mohanti, E. Bozkaya, M. Y. Naderi, B. Canberk, G. Secinti, and K. R. Chowdhury, "WiFED Mobile: WiFi Friendly Energy Delivery With Mobile Distributed Beamforming," *IEEE/ACM Transactions on Networking*, vol. 29, no. 3, pp. 1362–1375, 2021.
- [56] S. He, W. Ma, H. Dong, L. Xiao, and T. Jiang, "C-Cube: Rethinking Distributed Beamforming for Concurrent Charging in Backscatter Networks," *Proc. ACM Interact. Mob. Wearable Ubiquitous Technol.*, vol. 6, no. 4, jan 2023. [Online]. Available: https://doi.org/10.1145/3570342
- [57] S. Mohanti, E. Bozkaya, M. Y. Naderi, B. Canberk, G. Secinti, and K. R. Chowdhury, "WiFED Mobile: WiFi Friendly Energy Delivery With Mobile Distributed Beamforming," *IEEE/ACM Transactions on Networking*, vol. 29, no. 3, pp. 1362–1375, 2021.
- [58] K. W. Choi, L. Ginting, P. A. Rosyady, A. A. Aziz, and D. I. Kim, "Wireless-Powered Sensor Networks: How to Realize," *IEEE Transactions on Wireless Communications*, vol. 16, no. 1, pp. 221–234, 2017.
- [59] P. S. Yedavalli, T. Riihonen, X. Wang, and J. M. Rabaey, "Far-Field RF Wireless Power Transfer with Blind Adaptive Beamforming for Internet of Things Devices," *IEEE Access*, vol. 5, pp. 1743–1752, 2017.
- [60] X. Fan, H. Ding, S. Li, M. Sanzari, Y. Zhang, W. Trappe, Z. Han, and R. E. Howard, "Energy-Ball: Wireless Power Transfer for Batteryless Internet of Things through Distributed Beamforming," *Proc. ACM Interact. Mob. Wearable Ubiquitous Technol.*, vol. 2, no. 2, jul 2018. [Online]. Available: https://doi.org/10.1145/3214268
- [61] R. Wang, R. David, and D. R. Brown, "Feedback rate optimization in receiver-coordinated distributed transmit beamforming for wireless power transfer," in *Annual Conference on Information Sciences and Systems (CISS)*, 2015, pp. 1–6.
- [62] "GPSOCXO Specsheet," https://www.jackson-labs.com/assets/ downloads/GPSOCXO_Specsheet.pdf, accessed: 2022-03-08.
- [63] "OS364-13C Data Sheet," https://rfx.co.uk/uploads/Model-Data-Sheets/ OS364-13C.pdf, accessed: 2022-03-08.



Ankit Mittal received his B.Tech. degree in Electronics and Communication engineering from Dayalbagh Educational Institute, India in 2014 where he was also the recipient of Director's medal (Valedictorian Honor). Currently he is a Ph.D. candidate in the Energy Efficient Circuits and Systems Group, Electrical Engineering at Northeastern University, USA. Prior to joining Ph.D. program, he was a senior design engineer in NXP Semiconductors, India with a rich experience in SoC design and 5 memory testchip tapeout to his credit. His research

interests include power management integrated circuit design, ultra-low power biomedical circuits, ultra-low power RF radio design.



Ziyue Xu received the B.S degrees in electrical engineering from Anhui University, Hefei, China in 2016. In 2023, He received Ph.D. dgree from Northeastern University, Boston, MA, US. His research interests include power management integrated circuits design, RF design and energy harvester design. He is currently a staff electrical engineer in mobile solutions team at Skyworks Solutions, Inc., Andover, MA, US.



Kaden Du is a 3rd year undergraduate studying Electrical and Computer Engineer at Northeastern University. He joined the Energy Efficient Circuits and Systems group in the spring of 2022 due to interest in analog IC design, IoT, and low-power circuits. Apart from the Energy and Efficient Circuits and Systems Group, he is a project lead at the student led product led development studio. Kaden has experience at Notch Technologies as an EE Coop working on hardware and software for steerable antenna systems.



S. Shiva Kumar received the B.Tech. in Electrical Engineering from Gokaraju Rangaraju Institute of Engineering and Technology (GRIET) affiliated to Jawaharlal Nehru Technological University (JNTUK), India, in 2009. He received the M.Tech. in Power Electronics and Drives from Gokaraju Rangaraju Institute of Engineering and Technology affiliated to Jawaharlal Nehru Technological University (JNTUK), India, in 2011 and Ph.D. National Institute of Technology Rourkela (NITR). Currently working as a faculty in BIT Mesra Ranchi and

worked as an Exchange Visiting scholar at Northeastern University under Prof. Aatmesh Shrivastava. His research interest includes analysis and design of High Frequency Power Conversion Circuits, Power Factor Correction Circuits, SMPS, Electric drives, Soft-switching DC-DC converters, Hybrid electric vehicle and Energy harvesting RF waves using Beamforming techniques.



Aatmesh Shrivastava (S'12–M'15–SM'19) received his Ph.D. degree from the University of Virginia in 2014. Prior to his Ph.D., he worked as a senior design engineer at Texas Instruments, Bangalore from 2006 to 2010. From 2014 to 2016, he worked at an IoT start-up Everactive as a senior design director, where he was responsible for the research and development of the energy harvesting and power management solutions. In August 2016, he joined Northeastern University, where he is now working as an Associate Professor in the Electrical

and Computer Engineering Department. His research interests include self-powered and ultra-low power circuits and system, energy-harvesting and power-first system/computer architecture, analog computing, internet-of-things (IoT), ultra-low power bio-medical and neural circuits, exa-scale computing, and hardware security. He currently serves as an Associate Editor on the editorial board of the IEEE Transactions on Circuits and Systems Part I: Regular Papers (TCAS-I), IEEE Open Journal on Circuits and Systems (OJCAS), and as senior editor for IEEE Journal on Emerging and Selected Topics in Circuits and Systems (JETCAS). He was a recipient of DARPA Young Faculty Award in 2023, NSF CAREER Award in 2022, and Acorn Innovation Award from Mass Ventures in 2021, and the 2024 Faculty Fellow Award from the College of Engineering at Northeastern University.